Chemical Science

ROYAL SOCIETY OF CHEMISTRY

EDGE ARTICLE

View Article Online
View Journal | View Issue

Cite this: *Chem. Sci.*, 2025, **16**, 22498

All publication charges for this article have been paid for by the Royal Society of Chemistry

Received 23rd September 2025
Accepted 19th October 2025

DOI: 10.1039/d5sc07383a

rsc.li/chemical-science

Synthesis of wave-shaped Cu(II) porphyrin arrays and their electrocatalytic hydrogen evolution activity

Tao Jiang,†[a] Yuanbo Zhou,†[b] Tao Ye,†[c] Shihao Liu,[b] Ke Li,[b] Xiaohui Zhao,*[b] Zhongti Sun,[cd] Naoki Aratani,[e] Hiroko Yamada,[f] Fengxian Qiu,*[a] Jianming Pan,*[a] Toshiharu Teranishi[f] and Songlin Xue*[a]

The synthesis of wave-shaped porphyrin(2.1.2.1) arrays, including trimers and tetramers, was achieved for the first time through substitutional effects and building blocks. This enabled us to reveal the hydrogen evolution reaction (HER) capacity of the wave-shaped Cu(II) porphyrin(2.1.2.1) arrays. The trinuclear Cu(II) porphyrin(2.1.2.1) array exhibits remarkable HER capacity due to three catalytic Cu(II) ions and a π-ligand of porphyrin(2.1.2.1) array, resulting in lower overpotential, faster HER and charge transfer kinetics, and longer catalytic and charge transfer stability. In this study, we present a novel approach for the development of electrocatalytic molecular catalysts with multiple metal centres.

Introduction

Molecular catalysts have significant advantages in electrocatalysis thanks to their unique structures and tunability. These include (a) a well-defined structure; (b) structural engineerability; (c) tunable electronic properties; and (d) high atomic utilisation. They demonstrate outstanding performance in reactions such as the oxygen reduction reaction (ORR),[1a] the oxygen evolution reaction (OER),[1b] the hydrogen evolution reaction (HER)[1c] and electrocatalytic carbon dioxide reduction (ECO_2RR).[1d] These reactions have attracted significant interest in recent decades due to their potential for clean energy production and resource regeneration. Porphyrinoid ligands are famous and powerful N_4 ligands for creating monometallic complexes that act as molecular catalysts.[2] For instance, the mono-Cu(II) porphyrin(1.1.1.1) complex exhibits significant HER activity (Fig. 1a).[3]

In recent years, molecular catalysts containing two or more metal centres have attracted considerable interest due to their synergistic effects and multiple catalytic centres.[4] In 2018, Moore *et al.* reported that dinuclear Cu(II) fused porphyrins (Fig. 1a) exhibited enhanced hydrogen production with near-unity faradaic efficiency and a maximum turnover frequency exceeding 2 000 000 s^{-1}.[4a] Following this, in 2020 and 2023, the Apfel and Sarkar groups also reported other dinuclear Ni(II)[4b] and dinuclear Cu(II)[4c] porphyrins as HER molecular catalysts (Fig. 1a). However, to the best of our knowledge, molecular catalysts containing three or more metal catalytic centres have not yet been studied.

In our previous work, we reported the synthesis of dinuclear Cu(II) porphyrin (2.1.2.1) arrays using **DPB** and **TPB** (Scheme 1a) as building blocks.[5] However, we could not find any longer Cu(II) porphyrin (2.1.2.1) arrays, so we investigated the solubility of longer Cu(II) porphyrins. In this work, we focused on using the substitutional effect and a building block strategy to synthesize wave-shaped Cu(II) porphyrin(2.1.2.1) arrays (Fig. 1b). First, we report the design and synthesis of trinuclear Cu(II) porphyrin(2.1.2.1) arrays in ideal yields through simple condensation and coordination reactions. The molecular structure of the obtained porphyrin(2.1.2.1) arrays and their Cu(II) complexes was confirmed using high-resolution mass spectrometry (HR-MS), nuclear magnetic resonance (NMR) spectroscopy, electron paramagnetic resonance (EPR) spectroscopy and X-ray crystallography. Their optical properties and electronic structures were revealed using UV-Vis absorption and density functional theory (DFT) and time-dependent DFT (TD-DFT) calculations. Due to the presence of three catalytic Cu(II) ions, the trinuclear Cu(II) porphyrin arrays exhibit remarkable HER activity: lower overpotential, faster HER and charge

[a]*School of Chemistry and Chemical Engineering, Jiangsu University, 301 Xuefu Road, Zhenjiang 212013, China. E-mail: slxue@ujs.edu.cn*

[b]*School of Optical and Electronic Information, Jiangsu/Suzhou Key Laboratory of Biophotonics, International Joint Metacenter for Advanced Photonics and Electronics, Suzhou City University, Suzhou 215104, China*

[c]*School of Materials Science and Engineering, Jiangsu University, 301 Xuefu Road, Zhenjiang 212013, China*

[d]*Anhui Province Key Laboratory of Efficient Conversion and Solid-State Storage of Hydrogen & Electricity, Anhui University of Technology, 243002, Maanshan, China*

[e]*Division of Materials Science, Nara Institute of Science and Technology, 8916-5 Takayama-cho, Nara 630-0192, Japan*

[f]*Institute for Chemical Research, Kyoto University, Gokasho, Uji, Kyoto 611-0011, Japan*

† These authors contributed equally.

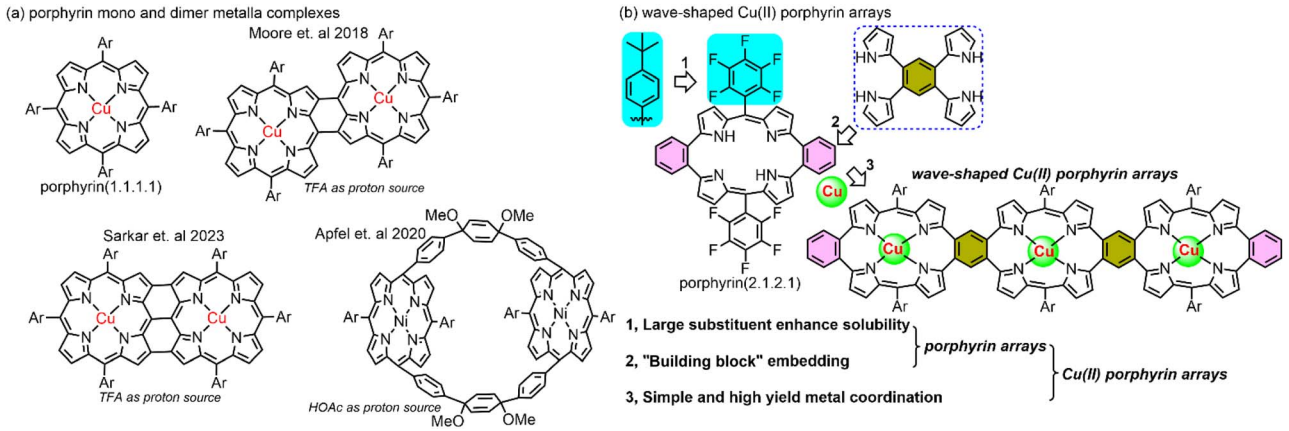

Fig. 1 (a) Examples of HER porphyrin mono-/multi-metal complexes; (b) our designed synthesis strategy for wave-shaped Cu(II) porphyrin arrays.

transfer kinetics, and longer catalytic stability than mono- and dinuclear Cu(II) porphyrin complexes.[3,5]

Results and discussion

In our previous work, we presented the porphyrin(2.1.2.1) copper dimer with pentafluorophenyl at the *meso* positions.[5a] Under the reaction conditions used, we could not identify the trimer or other oligomeric arrays. Therefore, in this study, we employed a large substituent to enhance solubility, in the hope of obtaining additional porphyrin(2.1.2.1) arrays (see Scheme 1a and the General synthesis section in the SI). The optimised condensation reaction of **DPB**, **TPB** and *tert*-butylbenzaldehyde was carried out in the presence of 70 mol% $BF_3{\cdot}OEt_2$ for three hours at room temperature under nitrogen, after which 2,3-dichloro-5,6-dicyano-1,4-benzoquinone (DDQ) was added to the reaction mixture and stirred for a further hour. The mixture was then purified using alumina and silica gel column

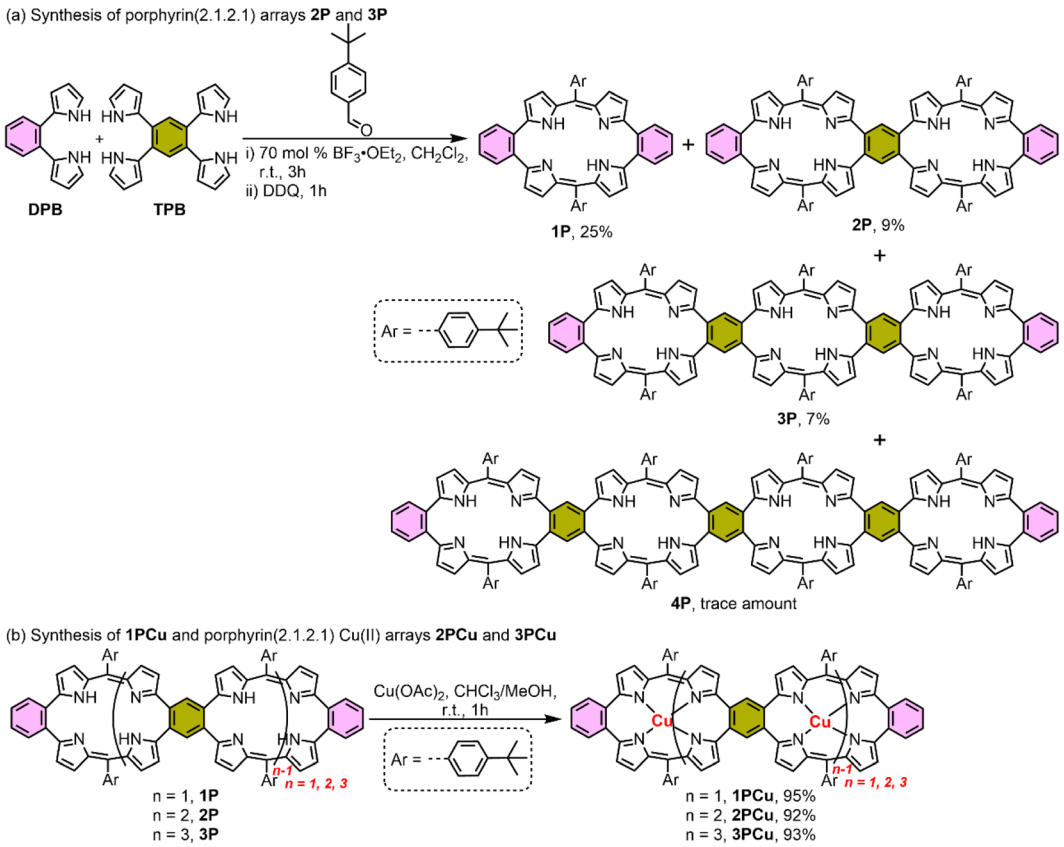

Scheme 1 Synthesis of wave-shaped porphyrin arrays and their Cu(II) complexes.

chromatography to obtain **1P** (25%), **2P** (9%) and **3P** (7%) at various yields. The larger tetramer **4P** was also observed as a trace product and characterised by HR-MS.

Ligands **2P**, **3P** and **4P** were characterized using HR-MS spectra. The HR-MS spectra of **2P**, **3P** and **4P** exhibit the corresponding molecular ion peaks at m/z = 1322.6709 (calcd for $C_{94}H_{82}N_8$ = 1322.6662 $[M]^+$) and m/z = 1944.9749 (calcd for $C_{138}H_{120}N_{12}$ = 1944.9758 $[M]^+$) and m/z = 2567.2697 (calcd for $C_{182}H_{158}N_{16}$ = 2567.2855 $[M]^+$) (Fig. S1–S3). As **4P** is present in trace amounts, the molecular structures of **2P** and **3P** were investigated by NMR spectroscopy. The ^{1}H NMR spectra of **2P** and **3P** reflect non-global aromaticity due to their highly bent structures. Both **2P** and **3P** exhibit two sets of β-H resonances between 6.6 and 6.2 ppm corresponding to the pyrrole units, and inner NH protons were observed at approximately 12.2 ppm (Fig. S4 and S5). The molecular structure of **2P** was determined using X-ray crystallography (Fig. 2). Unlike the reported planar and bent porphyrin(1.1.1.1) arrays,[6] the crystal structure of **2P** showed a wave-shaped molecular structure with two porphyrin(2.1.2.1) units. In **2P**, the two porphyrin(2.1.2.1) units have a bent structure similar to that of **1P**.[5] Despite multiple attempts, single crystals of **3P** and **4P** suitable for testing could not be obtained, likely due to their excessively large molecular structures. The molecular structures of **3P** and **4P** were investigated using DFT calculations and were found to be wave-shaped, similar to **2P** (Fig. S6 and S7).

The synthesized mono-porphyrin (**1P**) and wave-shaped porphyrin arrays (**2P** and **3P**) were reacted with $Cu(OAc)_2 \cdot H_2O$ in a $CHCl_3$/MeOH mixture solution under N_2 at room temperature for one hour, forming the metal complexes **1PCu**, **2PCu** and **3PCu** with isolated yields of over 90% (Scheme 1b and the Experimental section in the SI).[5] Characterization of these Cu(II) complexes revealed that the mono porphyrin **1P** and the wave-shaped porphyrin arrays **2P** and **3P** can act as tetrapyrrolic macrocyclic ligands. The molecular structures of **1PCu**, **2PCu** and **3PCu** were determined using HR-MS spectrometry and EPR spectroscopy. The HR-MS spectra of **1PCu**, **2PCu** and **3PCu** exhibit the corresponding molecular ion peaks at m/z = 762.2759 $[M + H]^+$ (calcd for $C_{50}H_{43}CuN_4$ = 762.2706 $[M + H]^+$), m/z = 1445.4961 $[M + H]^+$ (calcd for $C_{94}H_{79}Cu_2N_8$ = 1445.4942 $[M + H]^+$), and m/z = 2129.7170 $[M + H]^+$ (calcd for $C_{138}H_{115}Cu_3N_{12}$ = 2129.2502 $[M + H]^+$) (Fig. S8–S10). The Cu(II) ions in **1PCu**, **2PCu** and **3PCu** were confirmed by EPR spectroscopy in a CH_2Cl_2 solution, which showed clear Cu(II) signals (Fig. S11–S13 and 3).[3–5]

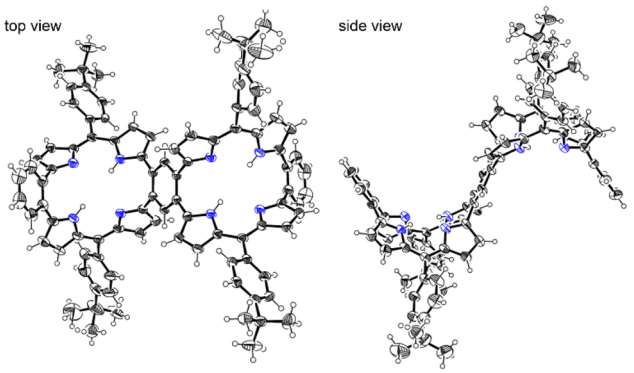

Fig. 2 X-ray crystal structure of **2P**. The thermal ellipsoids are given with 50% probability.

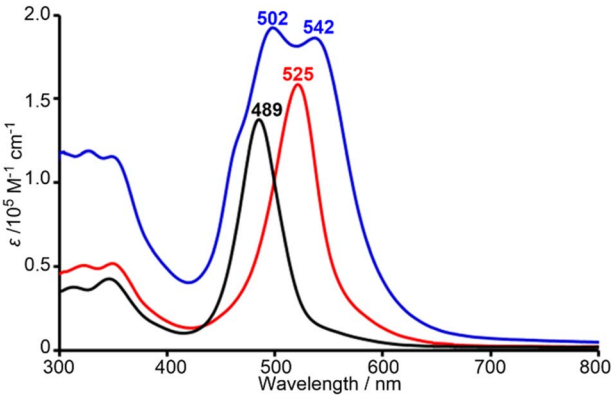

Fig. 3 UV-vis absorption spectra of **1PCu** (black line), **2PCu** (red line) and **3PCu** (blue line) in CH_2Cl_2 at 293 K.

UV-Vis absorption spectroscopy was employed to examine the optical and electronic properties of wave-shaped porphyrin arrays and their copper complexes. The UV-Vis absorption spectra of **2P** and **3P** were measured in a chloroform solution. Both **2P** and **3P** show a similar absorption profile to **1P**: they both exhibit a main absorption band at 450 and 455 nm, respectively (Fig. S14).[5] **1PCu** and **2PCu** both exhibited a red-shifted main absorption band at 489 and 525 nm respectively, compared to the main absorption bands of **1P** and **2P**. Interestingly, **3PCu** exhibited two red-shifted main absorption bands at 502 and 542 nm, resembling a combined absorption spectrum of **1PCu** and **2PCu**.[5] To gain a deeper understanding of the absorption and electronic structure of **3PCu**, DFT and TD-DFT calculations were carried out. Considering the frontier molecular orbitals, the TD-DFT calculations predicted that the absorption of **3PCu** would exhibit intramolecular charge transfer (ICT) characteristics.[7] For **3PCu**, TD-DFT predicted that the main absorption peaks at 550.41 nm (f = 0.0353) and 506.54 nm (f = 0.2846) correspond to β338 to β341 and β340 to β343 and α339 to α342, β300 to β347 and β300 to β348, respectively (Fig. S15–S17 and Table S1).

Two and three Cu centres of **2PCu** and **3PCu** have attracted our attention to investigate their catalytic properties.[2–4] A series of experiments were carried out using a three-electrode system in 1.0 M KOH to evaluate the alkaline HER activity of **1PCu@CNT**, **2PCu@CNT** and **3PCu@CNT**. Prior to the electrochemical performance tests, the **1PCu@CNT**, **2PCu@CNT** and **3PCu@CNT** samples were mixed with carbon nanotubes (CNTs) and loaded onto carbon cloth.[5a] The morphological and compositional characteristics of the samples were systematically investigated using scanning electron microscopy (SEM) and elemental mapping analysis (Fig. 4 and S18–S20). SEM images confirmed the formation of uniformly dispersed nanostructures on CNTs. Elemental mapping analysis revealed homogeneous spatial distributions of carbon (C), nitrogen (N), and copper (Cu) across the substrates.

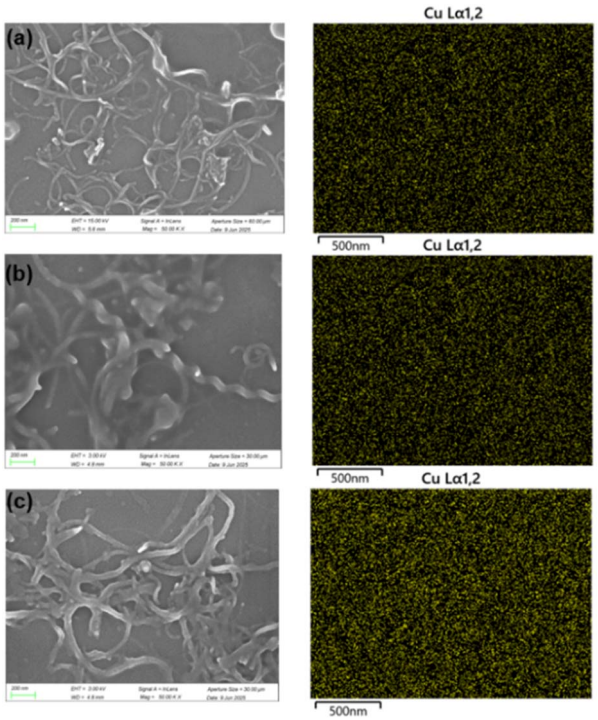

Fig. 4 (Left) SEM images and (right) EDS elemental mappings (Cu-L) of (a) **1PCu@CNT**, (b) **2PCu@CNT** and (c) **3PCu@CNT**.

High-resolution X-ray photoelectron spectroscopy (XPS) analysis of **1PCu@CNT**, **2PCu@CNT** and **3PCu@CNT** revealed characteristic Cu 2p peaks at binding energies of 935.1 ± 0.2 eV (Cu $2p_{3/2}$) and 955.2 ± 0.3 eV (Cu $2p_{1/2}$), as shown in Fig. 5. The XPS spectrum definitively identified carbon (C), nitrogen (N) and copper (Cu) as the constituent elements, showing close agreement with literature reports for Cu(II)-porphyrin(1.1.1.1)/CNT hybrid systems and Cu(II)-porphyrin(2.1.2.1)/CNT data. This confirms the stable +2 oxidation state of the copper centres.[5a]

Linear sweep voltammetry (LSV) of **1PCu@CNT**, **2PCu@CNT**, and **3PCu@CNT** was then conducted. As displayed in Fig. 6a, the HER activity of **2PCu@CNT** and **3PCu@CNT** catalysts all outperformed that of the **1PCu@CNT** catalyst. Among them, the **3PCu@CNT** catalyst exhibited the lowest overpotential to reach a current density of 10 mA cm^{-2}, which is 137 mV lower than that of the **1PCu@CNT** catalyst and 95 mV lower than that of the **2PCu@CNT** catalyst. And such activity also stands out among

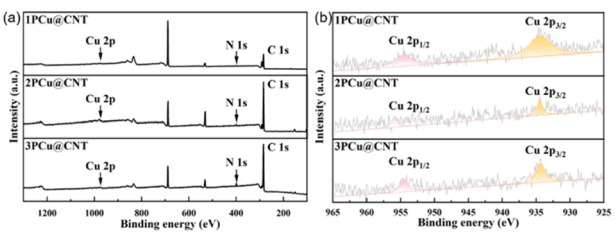

Fig. 5 (a) XPS survey spectra of **1PCu@CNT**, **2PCu@CNT** and **3PCu@CNT** and (b) the corresponding Cu 2p binding energy regions.

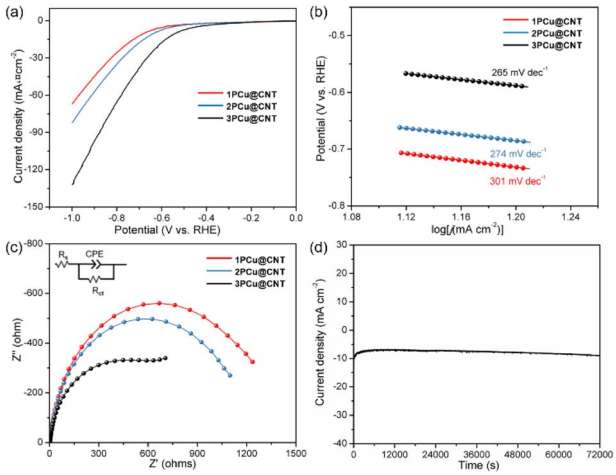

Fig. 6 (a) HER LSV curves of catalysts in 1.0 M KOH. (b) Tafel slope plots. (c) Nyquist plots. (d) *i*–*t* curves of **3PCu@CNT** in 1.0 M KOH at −0.6 V *vs.* RHE.

most of the metallic porphyrin-based catalysts.[5a,8,9] The HER activity is related to the strong π–π interaction between the extended conjugated skeleton of the porphyrin array, which can not only stabilize the catalyst surface, but also accelerate charge transfer.[5a,8,10] So the HER activity gradually increases as the porphyrin Cu(II) unit increases from 1 to 3.

To further probe the HER kinetics, the Tafel curves of **1PCu@CNT**, **2PCu@CNT**, and **3PCu@CNT** were plotted. As shown in Fig. 6b, the Tafel slopes of **2PCu@CNT** and **3PCu@CNT** are all smaller than that of **1PCu@CNT** (301 mV dec^{-1}). Among them, **3PCu@CNT** exhibits the smallest Tafel slope (265 mV dec^{-1}), proving its fastest HER kinetics. Electrochemical impedance spectroscopy (EIS) was also conducted to evaluate the conductivity of the circuit. As displayed in Fig. 6c, all the Nyquist plots of these samples exhibit a semicircle shape. Among them, the radius of **3PCu@CNT** is the smallest, which indicates its lowest charge transfer resistance (R_{ct}) and also proves its fastest charge transfer kinetics. In addition, cyclic voltammetry (CV) was performed at various scan rates to evaluate the double layer capacitance (C_{dl}). As exhibited in Fig. S21–S26, the C_{dl} values of **1PCu@CNT**, **2PCu@CNT**, and **3PCu@CNT** are 0.59 mF cm^{-2}, 0.72 mF cm^{-2}, and 1.34 mF cm^{-2}, respectively, indicating that **3PCu@CNT** possesses the highest electrochemical active surface area. Meanwhile, **3PCu@CNT** also maintained outstanding performance with no obvious current density change during 72 000 seconds of the HER stability test in 1.0 M KOH (Fig. 6d).

To further elucidate the difference in HER activity of wave-shaped Cu(II) porphyrin arrays, we use curved (**C-Cu**) and plane Cu (**P-Cu**) porphyrin complexes as catalytic units (Fig. S27) to do theoretical calculation. The first-principles method was executed to calculate the adsorption energy of hydrogen (ΔG_{*H}),[11–14] and computational details are displayed in the SI. The optimized **C-Cu** and **P-Cu** molecule models are shown in Fig. 7a and b, and the corresponding adsorbed hydrogen configurations are indicated in Fig. 7c–e. Their lowest adsorption energies of hydrogen are 1.84 and 2.03 eV on the **C-Cu** and

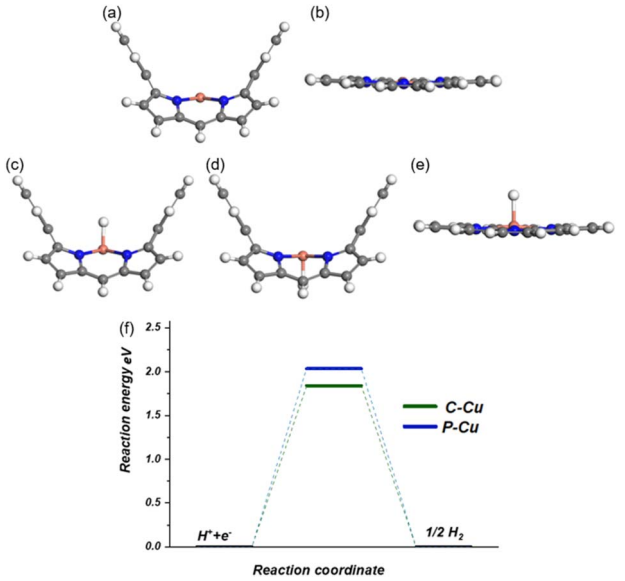

Fig. 7 The optimized configurations of C-Cu (a) and P-Cu (b); the optimized configurations of hydrogen on C-Cu (c and d) and P-Cu (e); the free energy change diagram of the HER on C-Cu and P-Cu (f). The orange, blue, grey, and white balls indicate Cu, N, C, and H atoms, respectively.

P-Cu catalysts, respectively, manifesting stronger H uptake on **C-Cu** than on **P-Cu**. The **C-Cu** molecule catalyst also exhibits shorter bond length between H and Cu atoms with 1.62 Å than **P-Cu** with 1.68 Å. Fig. 7f shows the free energy change of the HER. The **C-Cu** molecule catalyst demonstrates lower free energy change than **P-Cu** by 0.19 eV, indicating preferred HER performance. What's more, they possess the same potential determining step (PDS) with the capture of protons. Above all, the **C-Cu** molecule catalyst is significantly beneficial for the HER. A comparative table summarizing the HER performance of the developed **3PCu@CNT** catalyst alongside other recently reported porphyrin complex catalysts is given. The result indicates that **3PCu@CNT** is a potential molecular HER catalyst (Table S2).

Conclusions

In this study, we successfully synthesised wave-shaped porphyrin(2.1.2.1) arrays, comprising trimers and tetramers. Although the tetramer is a trace product, the yields of the dimer and trimer are ideal when they are isolated. Both the dimer and trimer exhibit a wavy molecular structure, as confirmed by X-ray crystallography. The tetramer also displays a longer wave-shaped molecular structure, as confirmed by DFT calculations. Due to their rich N_4 cavity, dinuclear and trinuclear Cu(II) porphyrin(2.1.2.1) arrays were obtained through coordination reactions with yields of over 90%. The optical properties and electronic structures of the Cu(II) porphyrin(2.1.2.1) arrays were revealed through UV-Vis absorption spectroscopy and DFT and TD-DFT calculations. As a reslut of π-ligand surface and three catalytic Cu(II) ions, the trinuclear Cu(II) porphyrin(2.1.2.1) array exhibits remarkable HER activity, with a lower overpotential, faster HER and charge transfer kinetics, and longer catalytic stability than mono- and dinuclear Cu(II) porphyrin(2.1.2.1) complexes. In this work, we have developed a new method for achieving electrocatalytic molecular catalysts with multiple metal centres.

Author contributions

S. X., X. Z., F. Q., and J. P. conceived the concept and prepared the manuscript with feedback from the other authors. T. J. performed the synthetic and characterization experiments. Y. Z., K. L., and S. L. performed the HER study. T. Y. and Z. S. performed the theoretical calculation. N. A. and H. Y. helped with HR-MS measurement and X-ray crystal structures. T. T. provided comments.

Conflicts of interest

The authors declare no competing financial interests.

Data availability

The data that support the findings of this study are available on request from the corresponding author, slxue@ujs.edu.cn (Prof. Dr. Songlin Xue), upon reasonable request.

CCDC 2490044 contains the supplementary crystallographic data for this paper.[15]

Supplementary information is available. See DOI: **https://doi.org/10.1039/d5sc07383a**.

Acknowledgements

This work was supported by the National Natural Science Foundation of China (22301108 and 22208128), the International Collaborative Research Program of the Institute for Chemical Research, Kyoto University (2025-110), the 2023 QINGLAN Project of Jiangsu Province of China, the Joint Training Master Postgraduate Research Innovation Program of Suzhou City University, the Suzhou Basic Research Project (SJC2023003), the China Postdoctoral Science Foundation (2023M731357) and the open project of Anhui Province Key Laboratory of Efficient Conversion and Solid-State Storage of Hydrogen & Electricity (ECSSHE2024KF03). This study was supported by the Joint Usage/Research Center [JURC, ICR, Kyoto University] by providing access to a Bruker Daltonics SolariX FT-ICR MS spectrometer. We are thankful for the theoretical calculations performed on the Northwest District of the Sugon National Supercomputer Center and the A6 Zone of the Beijing Super Cloud Computing Center, supported by PARATERA.

Notes and references

1 (*a*) M. Pegis, C. Wise, D. Martin and J. Mayer, *Chem. Rev.*, 2018, **118**, 2340; (*b*) X. Li, H. Lei, L. Xie, N. Wang, W. Zhang and R. Cao, *Acc. Chem. Res.*, 2022, **55**, 878; (*c*)

J. McAllister, N. Bandeira, J. McGlynn, A. Ganin, Y. Song, C. Bo and H. Miras, *Nat. Commun.*, 2019, **10**, 370; (*d*) L. Sun, V. Reddu, A. Fisher and X. Wang, *Energy Environ. Sci.*, 2020, **13**, 374.

2 (*a*) Z. Liang, H. Wang, H. Zheng, W. Zhang and R. Cao, *Chem. Soc. Rev.*, 2021, **50**, 2540; (*b*) T. Ouyang, H. Huang, J. Wang, D. Zhong and T. Lu, *Angew. Chem., Int. Ed.*, 2017, **56**, 738; (*c*) T. Ouyang, H. Wang, H. Huang, J. Wang, S. Guo, W. Liu, D. Zhong and T. Lu, *Angew. Chem., Int. Ed.*, 2018, **57**, 16480; (*d*) Z. Wei, H. Wang, C. Zhang, K. Xu, X. Lu and T. Lu, *Angew. Chem., Int. Ed.*, 2021, **60**, 16622–16627; (*e*) P. Wang, S. Guo, H. Wang, K. Chen, N. Zhang, Z. Zhang and T. Lu, *Nat. Commun.*, 2019, **10**, 3155.

3 X. Peng, M. Zhang, H. Qin, J. Han, Y. Xu, W. Li, X. Zhang, W. Zhang, U. Apfel and R. Cao, *Angew. Chem., Int. Ed.*, 2024, **63**, e202401074.

4 (*a*) D. Khusnutdinova, B. Wadsworth, M. Flores, A. Beiler, E. Cruz, Y. Zenkov and G. Moore, *ACS Catal.*, 2018, **8**, 9888; (*b*) J. Jokel, F. Schwer, M. Delius and U. Apfel, *Chem. Commun.*, 2020, **56**, 14179; (*c*) S. Chandra, A. Hazari, Q. Song, D. Hunger, N. Neuman, J. Slageren, E. Klemm and B. Sarkar, *ChemSusChem*, 2023, **16**, e202201146.

5 (*a*) Y. Dong, L. Qian, F. Chen, Y. Wang, T. Zhang, F. Qiu, T. Teranishi and S. Xue, *Chem. Commun.*, 2024, **60**, 3986; (*b*) S. Xue, X. Lv, N. Liu, Q. Zhang, H. Lei, R. Cao and F. Qiu, *Inorg. Chem.*, 2023, **62**, 1679; (*c*) J. Wu, X. Lv, Z. Xue, Y. Wang, F. Qiu and S. Xue, *Dalton Trans.*, 2025, **54**, 5255; (*d*) S. Xue, Y. Dong, T. Jiang, J. Wu, Y. Wei, L. Qian, X. Zhao, T. Zhang, F. Qiu and Q. Zuo, *Inorg. Chem.*, 2025, **64**, 6912; (*e*) T. Jiang, Y. Hu, S. Liang, F. Qiu, H. Huang, M. Zhou and S. Xue, *Dalton Trans.*, 2025, **54**, 8580.

6 (*a*) A. Ryan, A. Gehrold, R. Perusitti, M. Pintea, M. Fazekas, O. B. Locos, F. Blaikie and M. O. Senge, *Eur. J. Org Chem.*, 2011, 5817; (*b*) L. Liu, J. Liu, L. Zi, M. Zhou, L. Xu, Y. Rao, B. Yin, T. Higashino, A. Osuka and J. Song, *Org. Lett.*, 2025, **27**, 8088; (*c*) L. Zi, L. Liu, M. Zhou, L. Liu, B. Xiao, L. Xu, Y. Rao, B. Yin, J. Song and A. Osuka, *Angew. Chem., Int. Ed.*, 2024, **63**, e20231900; (*d*) Q. Pan, L. Liu, Y. Pan, M. Zhou, L. Xu, Y. Rao, B. Yin, J. Song and A. Osuka, *Org. Chem. Front.*, 2023, **10**, 5117; (*e*) J. Song, N. Aratani, H. Shinokubo and A. Osuka, *J. Am. Chem. Soc.*, 2010, **46**, 16356; (*f*) J. Song, N. Aratani, J. Heo, D. Kim, H. Shinokubo and A. Osuka, *J. Am. Chem. Soc.*, 2010, **34**, 11868; (*g*) L. Wang, Z. Liao, P. Lin, Y. Jia, L. Liu, L. Xu, M. Zhou, B. Yin, Y. Rao, A. Nakai, T. Tanaka, D. Shimizu, A. Osuka and J. Song, *Chem. Sci.*, 2024, **15**, 10207.

7 (*a*) S. Yang, C. Cao, J. Li, Z. Deng, S. Ni, J. Jian, Q. Tong, L. Dang and M. Li, *J. Phys. Chem. C*, 2022, **126**, 1076; (*b*) J. Hamza, J. Sharma, P. Karr, A. van der Est, F. D'Souza and P. Poddutoori, *J. Am. Chem. Soc.*, 2024, **146**, 25403; (*c*) M. Sun, P. Song, Y. Chen and F. Ma, *Chem. Phys. Lett.*, 2005, **416**, 94.

8 (*a*) W. Li, X. Peng, H. Qin, Y. Xu, J. Han, H. Lei and R. Cao, *Dalton Trans.*, 2024, **53**, 19121; (*b*) A. Ramuglia, M. Göbel, V. Budhija, M. Werheid, K. Ly, M. Schwalbe and I. Weidinger, *Inorg. Chem.*, 2023, **62**, 10232.

9 (*a*) X. Peng, J. Han, X. Li, G. Liu, Y. Xu, Y. Peng, S. Nie, W. Li, X. Li, Z. Chen, H. Peng, R. Cao and Y. Fang, *Chem. Commun.*, 2023, **59**, 10777; (*b*) A. Ramuglia, M. Göbel, V. Budhija, M. Werheid, K. Ly, M. Schwalbe and I. Weidinger, *Inorg. Chem.*, 2023, **62**, 10232.

10 (*a*) W. Zhang, M. Zhang, H. Wang, W. Zhang and M. Zhang, *Nano Res.*, 2024, **17**, 4850; (*b*) X. Su, F. Hong, Y. Fang, Y. Wen and B. Shan, *Angew. Chem., Int. Ed.*, 2025, **64**, e202422072.

11 L. Deng, L. Jin, L. Yang, C. Feng, A. Tao, X. Jia, Z. Geng, C. Zhang, X. Cui and J. Shi, *eScience*, 2025, **5**, 100353.

12 H. Han, J. Choi, M. Son and K. Kim, *eScience*, 2024, **4**, 100204.

13 B. Han and F. Li, *J. Mater. Inf.*, 2023, **3**, 24.

14 C. Zhang, S. Qin, H. Gao and P. Jin, *J. Mater. Inf.*, 2024, **4**, 1.

15 CCDC 2490044: Experimental Crystal Structure Determination, 2025, DOI: **10.5517/ccdc.csd.cc2pl30f**.